School of Natural Sciences and Mathematics

Tunable Organic PV Parallel Tandem with Ionic Gating

UT Dallas Author(s):

Alexander B. Cook
Jonathan D. Yuen
Anvar Zakhidov

Citation:

Saranin, Danila, Artur Ishteev, Alexander B. Cook, Jonathan D. Yuen, et al. 2017. "Tunable organic PV parallel tandem with ionic gating." Journal of Renewable and Sustainable Energy 9(2), doi:10.1063/1.4979900

Tunable organic PV parallel tandem with ionic gating

Danila Saranin,[1,3,a)] Artur Ishteev,[1] Alexander B. Cook,[2] Jonathan D. Yuen,[2] Denis Kuznetsov,[1] Marina Orlova,[3] Sergey Didenko,[3] and Anvar Zakhidov[1,2,a)]

[1]*Energy Efficiency Center, National University of Science and Technology MISiS, Moscow 119049, Russia*
[2]*Physics Department and The NanoTech Institute, The University of Texas at Dallas, Richardson 75080, USA*
[3]*Department of Semiconductor Electronics and Physics of Semiconductor Devices, National University of Science and Technology MISiS, Moscow 119049, Russia*

(Received 25 October 2016; accepted 24 February 2017; published online 7 April 2017)

A novel type of tunable organic photovoltaic (OPV) tandem device with ionic gating by *in-situ* ionic liquid is presented. This device is comprised of two solution-processed polymeric OPV cells connected in parallel by a dry-laminated transparent multiwall carbon nanotube (MWCNT) interlayer. The interlayer MWCNT of this 3-terminal tandem device plays a role of a common electrode with a Fermi level that can be tuned via ionic gating to turn it into a common cathode, collecting photo-generated electrons from both sub-cells. Ionic gating employs electric double layer charging of the MWCNT in order to lower the work function of the common CNT electrode and increase its n-type conductivity. This tandem device is fabricated in ambient conditions via dry-lamination of MWCNT transparent sheets The new results demonstrating the different regimes of ionic gating at low, medium, and high gating voltages V_{gate} are presented, showing the optimal doping of the MWCNT, then favorable doping of acceptor PCBM ([6,6]-phenyl-C_{61}-butyric acid methyl ester), followed by the deterioration of performance at V_{gate} over the threshold voltage when doping of polymeric layers of sub-cell OPVs starts taking place. The doping of PCBM and polymers is additionally confirmed by the change in the charging and discharging current dynamics at high V_{gate} above the threshold. *Published by AIP Publishing*. [http://dx.doi.org/10.1063/1.4979900]

INTRODUCTION

Polymer semiconductors are the leading organic photovoltaic (OPV) materials due to their high absorptivity, good transport properties, flexibility, and compatibility with temperature sensitive substrates. The power conversion efficiencies (PCE), η, of OPV devices have jumped significantly in the past few years, with single cell efficiencies as high as 9%–11%,[1–3] making them an increasingly viable energy technology.

Despite the improvements in η, the quite thin active layer thicknesses of the typical single junction OPV cells limit light absorption[4,5] and hinder reliable fabrication. Additionally, the spectral width of light absorption of each polymer is limited compared to inorganic materials. Pairing polymers of differing spectral sensitivities of each single PV (photovoltaics) sub-cell into an optimal tandem device[6] bypasses these difficulties, making the correct choice of proper tandem architectures[7] a necessary innovation.

In-series OPV tandem devices are the most common architecture used in the current state of the art monolithic tandem devices.[8,9] In this design, an electron transport material, an optional metallic recombination interconnection layer, and a hole transport layer connect two

[a)]Authors to whom correspondence should be addressed. Electronic addresses: zakhidov@utdallas.edu and danilasaranin@gmail.com

independent photoactive layers called sub-cells in a two terminal configuration. Linking sub-cells in a series configuration increases the open circuit voltage of the combination device, but only a minimal current of two sub-cells can be conducted (this condition requires balancing of photocurrents of both the sub-cells).[10] Some groups have succeeded with doped transport layers,[11–13] but more groups have used particles of gold or silver to aid the recombination of holes and electrons in the interlayer.[14–17] Various types of interconnection layers discussed in reviews include inorganic and hybrid interconnections.[18,19]

In contrast, a parallel tandem interlayer with three terminal[20–25] or four terminal configurations[26–28] requires a high conductivity common 3-d electrode, either an anode or a cathode, joining the two sub-cell OPV devices via a transparent conductive interconnect (advantages and specifications of both the types of connections are discussed in Refs. 20–22 and 29–32). This interlayer must be highly optically transparent (which also limits in-series tandem interlayers, containing sometimes non-percolated metallic particles, e.g., of Ag as recombination centers), and even more important is this condition for the parallel tandem interlayer, since it acts as a 3d common electrode, usually composed of thin, continuous metal electrodes. Carbon nanotube (CNT) sheets show higher optical transparency than metal layers.[33] The concept of using transparent CNT sheets as the interlayer electrode, acting as a charge collector in monolithic, parallel tandem devices, has been successfully demonstrated earlier.[20–22]

Previous efforts featured monolithic, parallel, tandem OPV devices with CNT sheets functioning as positive charges collectors; in other words, a 3-d electrode was an interlayer common anode.[20,21] These methods for making monolithic OPV tandem devices require special care to avoid shorting of one or both sub-cells or damaging preceding layers when depositing later layers. The new method described in this paper makes tandem fabrication much easier by placing two CNT electrodes on top of the polymeric active layers of each of the two sub-cell OPVs and then joining the two separate devices together (after the insertion of ionic liquid on top of multiwall carbon nanotube (MWCNT) laminated stripes) in a face to face manner by pressing them mechanically and connecting two MWCNT electrodes soaked by ionic liquid on top of each other as shown in Figures 1(b) and 3. This method is remarkable as the whole tandem device, including air-stable MWCNT cathodes, can be fabricated entirely in ambient conditions employing only dry lamination (for MWCNT sheets) and solution processing (for polymers), with no need for any vacuum deposition.[35–37]

Multiwall CNT sheets (scanning electron microscopy (SEM) microscopy images presented in Figs. 2(a) and 2(b), studied here (in contrast to single wall CNTs of our earlier work[34] on tandem devices)) are not intrinsically good cathodes since they have a high work function (in the range of 5.1–5.4 eV, depending on synthesis conditions), and therefore, they require n-type doping to raise their Fermi level and thus to decrease the work function[33,34] in order to collect electrons from the photoactive region of a solar cell.[20] Electric double layer charging (EDLC) in an electrolyte, such as an ionic liquid, can be used to achieve the shift of the work function of CNT electrodes.[34–37] This concept is used in our work for tandem architecture (see also

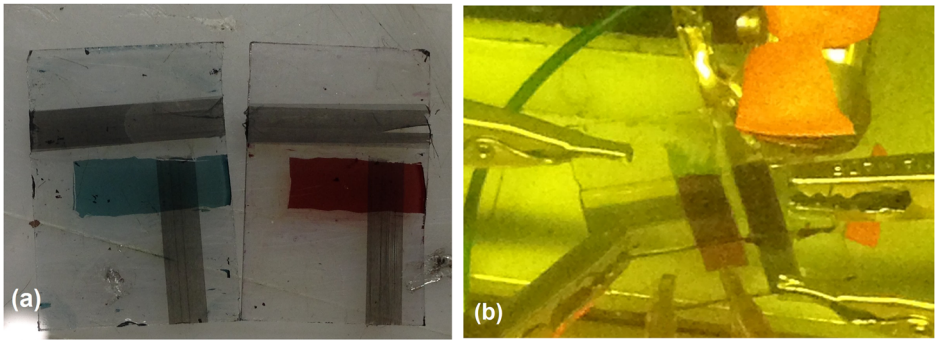

FIG. 1. (a) Separate OPV sub-cells with laminated MWCNT semi-transparent cathodes and the MWCNT gate (a horizontal stripe). (b) Assembled tandem device by face-to face connection of sub-cells after ionic liquid insertion.

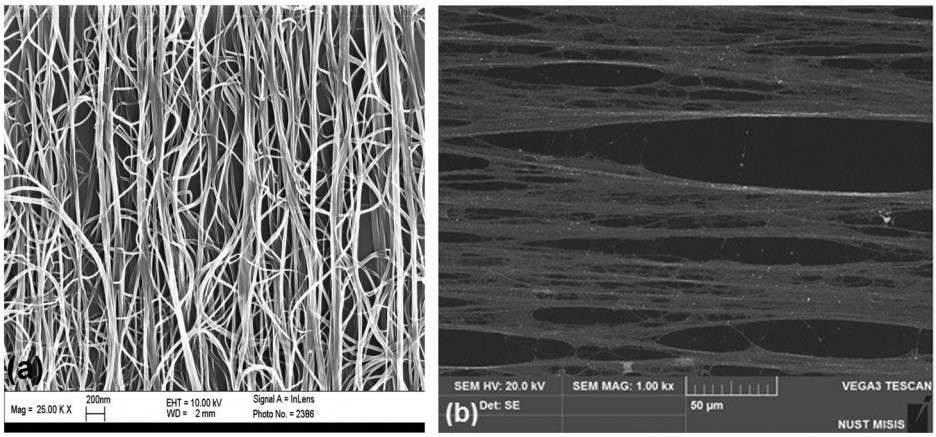

FIG. 2. (a) SEM image of densified MWCNTs at a large magnification, showing the highly porous CNT bundle network, accessible for ionic liquid. (b) Free standing SEM image of multiwall carbon nanotubes.

Refs. 36 and 37), as it is shown in Figure 3, where porous MWCNT electrodes of two sub-cells soaked with ionic liquid form one common electrode of the tandem device (common 3-d electrode) and another MWCT (multi-walled carbon nanotubes) electrode named the "counter-electrode" or gate is placed near the device pixel for EDLC by applying a gate voltage V_{gate} to it, as shown in the lower part of Figure 3.

So, in this work, we used only MWCNTs in contrast to Ref. 37 which used SWCNTs (single-walled carbon nanotubes) as common electrodes. Scanning Electron Microscopy (SEM) images of free-standing MWCNTs are presented in Figures 2(a) and 2(b) on different zoom scales. The advantages of using MWCNTs are obvious: our MWCNTs are free-standing mechanically strong aerogels, which can be easily dry-span from vertically oriented MWCNT forests[40,41] and then dry-laminated, just like a scotch tape to any surface without any need for transfer processes from support membranes (as done in the case of SWCNTs, used in Ref. 37). Such MWCNTs provide 3-dimensional charge collection in OPVs[42] and can be used as top-laminated charge collectors in OPVs and OLEDs (organic light-emitting diodes),[43] but they have initially a high sheet resistance Rsh ~500–1000 Ω/sq in the as-synthesized undoped state. Therefore, one of the motivations of our present research is to find out if ionic gating can decrease Rsh to the level of Rsh $< 100\,\Omega$/sq, required for PV applications, at reasonably high optical transmission T $> 75\%$–80%. While SWCNTs have 2/3 of them, after synthesis, as semiconducting tubes, which can be doped by ionic gating to the low Rsh state at still high T, the MWCNTs are from the beginning all metallic. Ionic gating changes the work function of MWCNTs in the wide range of ± 0.5–0.9 eV at small $V_{gate} < 1.5$ eV, but it was not clear what will be the changes at higher V_{gate}, when the larger raise of the Fermi level can induce doping of OPV layers, adjacent to the

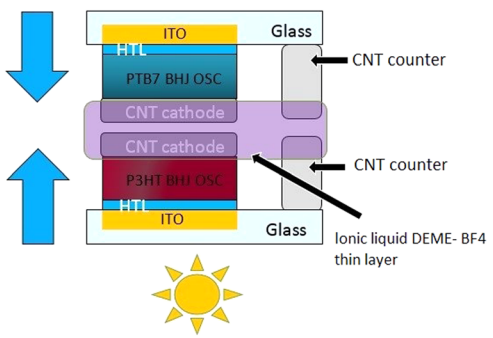

FIG. 3. Tandem device cross-sectional schematics with top P3HT and bottom PTB7 sub-cells with laminated MWCNTs soaked in ionic liquid.

MWCNT porous electrode. Indeed, we demonstrate here that gating MWCNTs at higher V_{gate} can induce n-doping of acceptor PCBM ([6,6]-phenyl-C_{61}-butyric acid methyl ester) in OPV and even other layers, while Rsh is lowered to required low values.

The fabrication and lamination process was used for building the ionically gated tandem OPV—separate sub-cells with deposited CNT cathodes and counter electrodes.

The simple fabrication process used for building the ionically gated tandem OPV is clearly shown in Figs. 1 and 3: separate OPV sub-cells with dry lamination deposited CNT cathodes and CNT counter electrodes and soaked in ionic liquid are placed on top of each other and pressed to spread ionic liquid uniformly. Ions of proper charge signs will start penetrating the pores in the MWCNT 3D mesh upon gating voltage. The ionic layer on the surface of CNTs with electronic charge injected to CNTs from leads will form EDLC[33–35] which will keep spreading with increased V_{gate}.

As described in Refs. 36 and 37 and depicted in Figure 4, when the gate voltage (V_{gate}) is increased, the work function of the CNT common electrode is decreased (by the raised Fermi level), creating electrode asymmetry and forming a built-in electric field for better charge collection. This prevents hole collection on CNTs from the OPV's donor polymer in favor of collecting electrons from the OPV's acceptor, and each single sub-cell device is thus tuned "ON" changing from the inefficient photo-resistor (which has two electrodes with a similarly high work function, ITO and MWCTs) into a photodiode[36,37] with rectifying behavior due to asymmetry between "ITO and n-MWCNT." It should also be noted that the energy used to charge the EDLC on the CNT interlayer of our tunable tandem device and the power spent for charging and also for power lost due to gate leakage currents are minuscular, i.e., on the micro-watt scale (as seen in charging current curves in Fig. 17 and figures in the supplementary material) as compared to 100 s of mW/cm^2 scale power photogenerated by the "turned ON" solar cell.[36,37] Ionic gating of CNT electrodes has a large effect on the work function due to the low electronic density of states in 1-D CNTs and the high surface area to volume ratio in the here studied multiwall CNT electrodes. Similar methods of EDLC the gate have been used to enhance a Schottky barrier at the interface of CNTs with n-Si.[38,39]

REPRESENTATIVE RESULTS

A tandem device formed from different donor polymers, BHJ (bulk hetero junction) active layers, particularly polymers of significantly different bandgaps (approximately 2 eV for the P3HT sub cell and 1.7 eV for the PTB7 sub-cell), is of practical interest as this device can absorb the largest spectral range of light. In this device structure, the PTB7/PCBM sub-cell is the back cell and P3HT/PCBM is the front sub-cell. This is intended to absorb the greatest amount of light as the P3HT sub-cell is largely transparent to the longer wavelength light absorbed by the PTB7 sub-cell. For the sake of clarity, the solar cell parameters V_{OC}, J_{SC}, FF

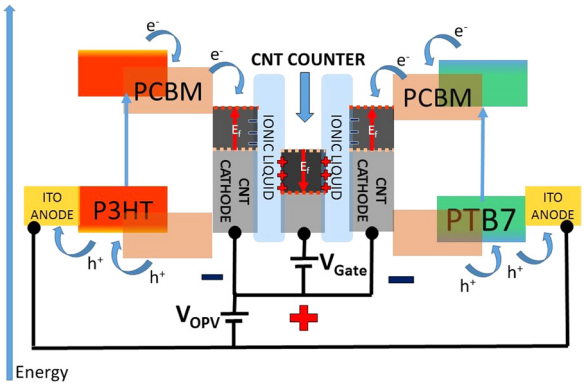

FIG. 4. Tunable Ionically gated Tandem Device Band structure and Electrical Diagram, where color boxes describe the HOMO/LUMO levels of each sub- cell, red dot line shows the Fermi level position of CNT electrodes, and red arrow depicts the shifting or lowering of the Fermi level upon ionic gating.

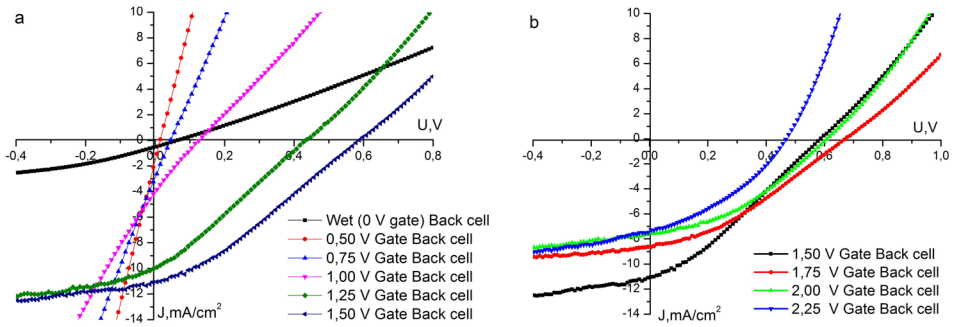

FIG. 5. (a) IV curves for the PTB7 back cell before peak characteristics at the 1.5 V gate; (b) IV curves for the PTB7 back cell after peak characteristics at the 1.5 V gate in which the back (PTB7) cell shows its best performance.

(fill factor), and η (PCE) will be decorated with a superscript Tandem, Front, and Back when referring to the tandem, front, or back cell, respectively. Bias between the CNT counter electrode and the cell's CNT cathodes is marked as V_{gate}, respectively, and its value varied from 0 to 1.5 V and then more to 2.25 V with a step of 0.25 V.

A selection of current voltage I-V curves for each device is presented in Figs. 5–8, and the extracted solar cell parameters are presented in Tables I and II (Table III is given in the supplementary material data part). During testing of the device under 1.5 AM G illumination, each sub-cell was first measured separately, so the P3HT sub-cell was tested as the top and front cell and the PTB7 sub-cell as the bottom and back cell under imitation of light shading in a monolithic configuration. It has been observed that the PTB7/PCBM sub-cell (back cell of a tandem device) turned "ON" at a much lower gating V_{gate} than the P3HT/PCBM sub-cell (front cell of a tandem device). Fig. 5 shows that the PTB7 cell begins to turn "ON" at $V_{gate} = 0.5$ V and peaks around $V_{gate} = 1.5$–1.75 V. The front sub-cell shows signs of turning "ON" at a higher gating potential around $V_{gate} = 1.0$ V but does not fully turn "ON" below $V_{gate} = 2.0$ V. The resulting tandem V_{OC} and FF mimic the behavior of the worse sub-cell, being slightly higher than the front sub-cell for $V_{Gate} < 2.0$ V and slightly higher than the back cell for $V_{gate} > 2.0$ V. At the same time, the resulting tandem current (which in the ideal case should be a sum of two sub-cells) tandem J_{SC} is far less than the sum of Front J_{SC} and Back J_{SC} for $V_{gate} < 1.5$ V, after which point, the current addition is quite good. Tandem PCE, η^T, is smaller than the greater PCE of the Front cell η or PCE of Back cell η of gating for all V_{gate} except those peak values at $V_{gate} = 1.5$ and 1.75 V.

The poor addition of currents to the total current of the tandem device and the increase in the efficiency of the tandem device for low V_{gate} appear to be due to the effect of the front sub-cell acting as a shunt in its yet "OFF" state, while the back cell is already "switched ON" by the ionic DLC gate into a good PV diode. This is seen from the still linear curves of the front cell and the tandem device at $V_{gate} = 1.5$ V in Figures 6 and 7. Conversely, after the

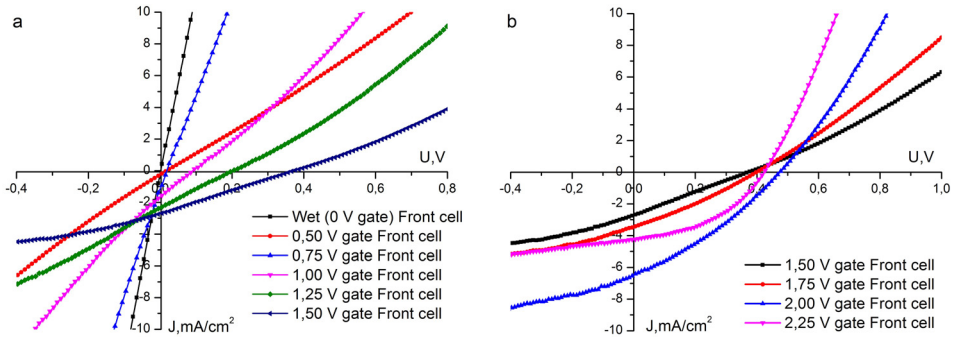

FIG. 6. (a) IV curves of the P3HT front cell up to the 1.5 V gate and (b) IV curves of the P3HT front cell up to 2.25 V, in which the front (P3HT) cell shows its best performance at 2.00 V.

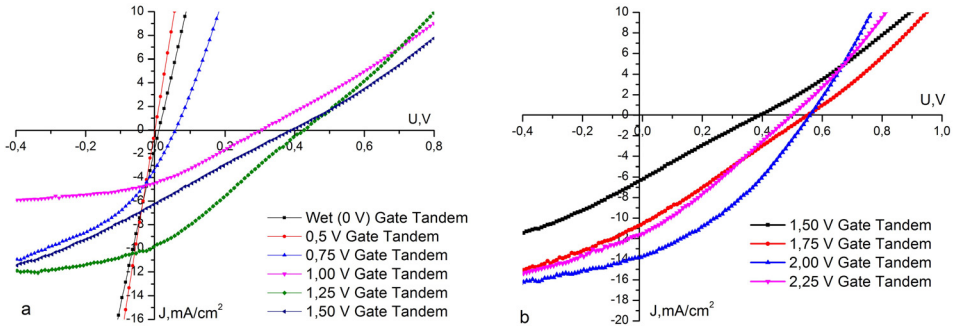

FIG. 7. (a) Tandem IV curves up to the 1.5 V gate and (b) tandem IV curves up to 2.25 V, where IV curve for a $V_{gate} <$ 1.5 V in which the tandem device works in the PTB7 sub-cell full contributes mostly to tandem operation (a) and higher V_{gate} (2.00 V) in which the front (P3HT) cell and the tandem device show its best performance (b).

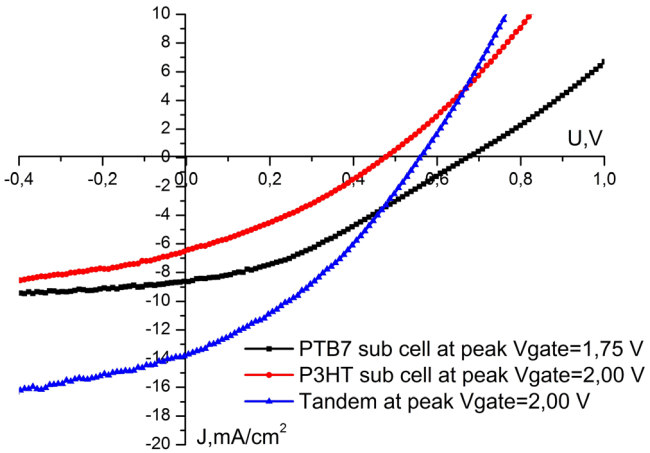

FIG. 8. Tandem device and front and back sub-cell best IV curves at their peak V_{gate}.

TABLE I. Back ionically gated PTB7 cell (in tandem measurements) output parameters.

Ugate (V)	Uoc (V)	Jsc (mA/cm^2)	FF	Efficiency (%)	Rs (Ω cm^2)	Rsh (Ω cm^2)
0	0.065	0.489	0.275	8.82×10^{-03}		
0.5	0.015	1.047	0.329	0.0051	…	…
0.75	0.045	2.618	0.273	0.032	8.15	1653.00
1.0	0.125	3.85	0.239	0.115	22.32	2900.58
1.25	0.437	4.36	0.267	0.510	26.87	3642.78
1.5	0.587	11.03	0.301	0.909	33.35	5241.02
1.75	0.668	8.63	0.338	1.954	29.11	9483.39
2.0	0.607	7.50	0.383	1.751	28.87	1665.03
2.25	0.467	7.29	0.368	1.255	8.02	1715.13

PTB7/PCBM back cell has degraded (at $V_{gate} = 2.25$ V), it still maintains diode characteristics, as shown in the curve in Figure 5(b) and thus does not act as a shunt. This results in the addition of J_{SC} to total current, but Tandem V^T_{OC}, FF, and η are reduced due to the low Back cell V_{OC}. While the ionic gating process draws robustness from its simplicity, there are variations due to the manual processing and batch-to-batch variations in materials. This can result in shifts in the turn on voltage of ± 0.25 V and peak efficiency by $\pm 0.5\%$. This variation can be decreased with a more automated process.

TABLE II. Monolithic ionically gated tandem output parameters.

Ugate (V)	Uoc (V)	Jsc (mA/cm^2)	FF	Efficiency (%)	Rs (Ω cm^2)	Rsh (Ω cm^2)
0	0.01304	0.72238	0.327	0.00356	…	…
0.5	0.0151	1.1605	0.327	0.0057	…	…
0.75	0.035	3.055	0.318	0.0341	…	…
1.0	0.3065	4.42	0.276	0.374	20.13	2130.76
1.25	0.427	5.034	0.270	0.582	27.68	2267.33
1.5	0.396	6.17	0.241	0.591	29.89	4835.96
1.75	0.547	10.47	0.263	1.514	24.60	12197.85
2.0	0.557	12.98	0.336	2.430	19.65	17974.23
2.25	0.497	12.14	0.298	1.798	14.14	14704.40

As it was noticed before, the P3HT front cell started to improve its output characteristics only at high V_{gate} (2.00 V) in which the front (P3HT) cell shows its best performance (Table II). Also, the regime of front cell operation shows meaningful IV parameters only after 1.25 V of V_{gate}, as it is shown in Figure 7(a), while the PTB7 back cell is closer to the peak performance at the same bias between common and counter CNTs.

Accordingly, the results of the output IV parameters of front and back cells extracted in the two regimes of tandem operation are observed. The first one "PTB7 sub-cell full on tandem regimes" shows tandem behavior at V_{gate} below 1.5 V, when the PTB7 sub-cell strongly gains its power. Another one "P3HT sub-cell full on tandem regime" shows tandem behavior after >1.5 V Gate, when PTB7 sub-cell performance becomes poorer and P3HT shows its best. So, for these depicted regimes of tandem operation, it is possible to conclude that at $V_{gate} < 1.5$ V, the back cell pulls and gains its operation, and after 1.5 V, P3HT increases its contribution (as is presented in Figures 7(a), 7(b), and Table III (supplementary material)).

To fix the difference in the sub-cells, the operation plot of best IV curves is presented in Figure 8, where for each sub-cell and tandem, best IV curves are presented, respectively, at the peak V gate.

The further increase in gate voltage resulted in quite interesting behavior, which will be analyzed below. Indeed, when Vg exceeded the certain threshold value of Vth, the improvement of performance in terms of higher Jsc and better FF has stopped and in fact reversed.

As shown in Figures 9–12, the I-V curves of the PTB7-CNT-P3HT tandem device are declining after V_{gate} of 2.00 V in contrast to PTB7 single sub-cell performance which started to

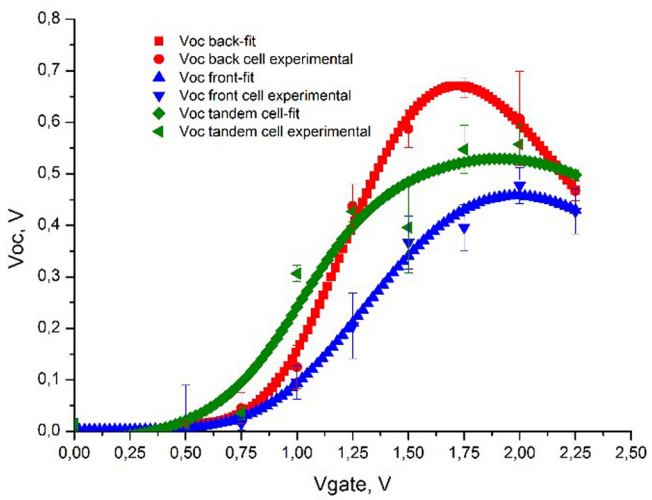

FIG. 9. Comparison of Voc dependencies of Vgate of each presented device with the Ey bar.

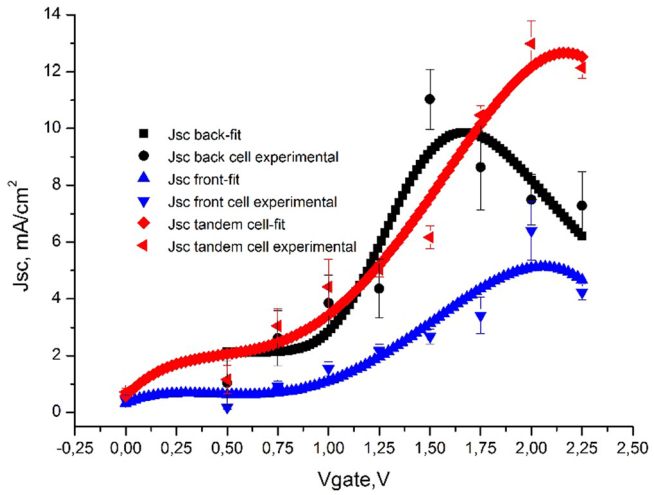

FIG. 10. Comparison of Jsc dependencies of Vgate of each presented device with the Ey bar.

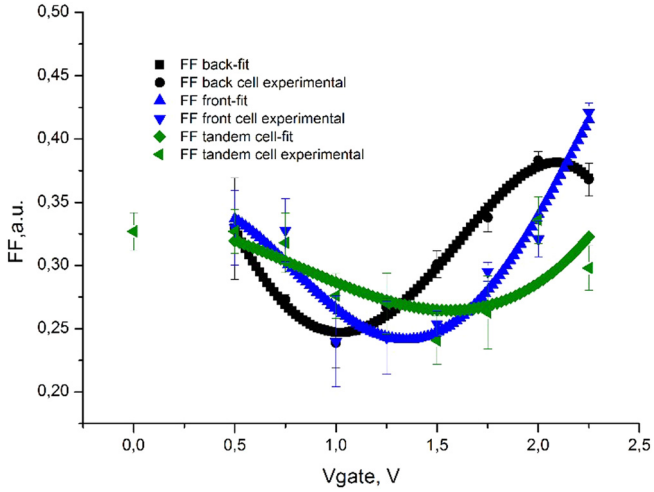

FIG. 11. Comparison of FF dependencies of Vgate of each presented device with the Ey bar.

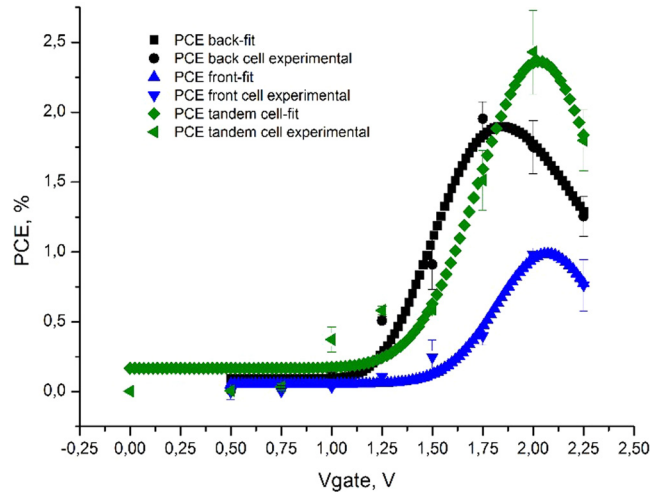

FIG. 12. Comparison of PCE dependencies of Vgate of each presented device with the Ey bar.

degrade at high V_{gate}. Figs. 9–12 present various dependencies with error bars which were calculated from 3 series of tandem devices for comparison with the best sample presented before with its output JV curves.

DISCUSSIONS

We have investigated different regimes of ionic gating of the CNT electrode: at low, medium and high gate voltages Vg. While we have taken measurements over a large range of the Vgate, we shall only focus on two important points during gating of the tandem devices—the point where the photodiode effects have just started to appear in the sub-cells (the device "turns ON"), and the optimal point at which the sub-cells are at their best performance. At large V_{gate}, the sub-cell performance deteriorates, and all the parameters are decreased. For the sake of clarity, Jsc, Voc, and FF will be marked by superscripts, defining top, bottom, and total values.

(a) At low V_{gate} ($V_{gate} < 1.5$ V that we have already studied earlier in Refs. 35–37), the gate induces the EDLC doping of the CNT, raising its Fermi level and increasing Voc from ∼0 V to ∼0.3–0.4 V. The Isc increases due to better charge collection by the n-doped CNT (via EDLC), at this relatively small Vg.

(b) at medium V_{gate}, the porous CNT network is already filled with ions that equilibrate the electronic EDLC charges on the CNT conduction band and the ions start penetrating further into the polymeric part, i.e., into BHJ, and beginning the n-doping of the PCBM acceptors (by charge injection from the already n-type CNT). This doping spread to the ETL (electron transport layer) part of BHJ starts when Ef of the CNT is raised high enough (by $V_{gate} > 1.5$ V) and reaches the LUMO level of PCBM, making it energetically favorable for electrons to be transferred from the CNT to PCBM. This n-doping of PCBM leads to the formation of the low resistive, ohmic interface between n-doped CNTs and the formation of the n-doped PCBM layer at the interface with the CNT. Moreover the n-doped PCBM layer (shown at x depth with $x < L$) creates an "n-I" build-up junction with the undoped, Intrinsic, i-part of PCBM at the L-x part, and thus, a favorable pulling internal electric field is created for electrons, further improving the performance of OPV by better charge collection and providing a better FF. In this medium regime, the performance of the whole tandem device increases further due to the favorable partial n-doping of the acceptor.

(c) The high V_{gate} gating regime $1.75\ V < V_{gate} < 2.25$ V is a new regime studied here with the example of PTB7, i.e., low gap and low LUMO donor polymer of BHJ. In this regime, the EDLC on the PCBM acceptor occupies the whole width L of BHJ, and when the Fermi level of the CNT is raised above the LUMO of PTB7, the electrons can be injected into donor polymer chains and the whole body of BHJ becomes n-doped, decreasing the absorption of light in doped parts of PTB7.

Now, when the steps of EDLC doping and changes of R_{ser} and R_{sh} are qualitatively understood, let us turn to the dynamics of J-V curves, which changes with the increase in Vg. The obtained non-trivial results highlight a few considerations when designing parallel tandem solar cells, dynamically tunable by gating. Notably, if one of the sub-cells is performing poorly (due to delayed switching "ON" into their diode state), then the total tandem performance is negatively affected. The results show that there are two main effects. If one sub-cell is shorted (not yet converted by EDLC into a photodiode state), e.g., shows ohmic behavior, the tandem FF^T will be no higher than the FF of the "bad" sub-cell. Tandem J_{SC} and V_{OC} will be similarly negatively affected. This is the case when V_{gate} is low and the P3HT/PCBM (lower) sub-cell has not turned "ON" into a diode yet, while a top sub-cell is already turned ON.

Conversely, if one sub-cell has good diode properties, but low V_{OC} or J_{SC}, then Tandem J_{SC} is nearly the sum of Front cell J_{SC} and Back cell J_{SC}. However, if there is a large difference between each sub-cell V_{OC}, then Tandem V_{OC} is nearly equivalent to the lesser V_{OC}. This performance is demonstrated when e.g., V_{gate} is high and the PTB7/PCBM cell has turned OFF. The total Tandem η (PCE) can be somewhat higher in this case but is still likely to be less than that of the better sub-cell alone.

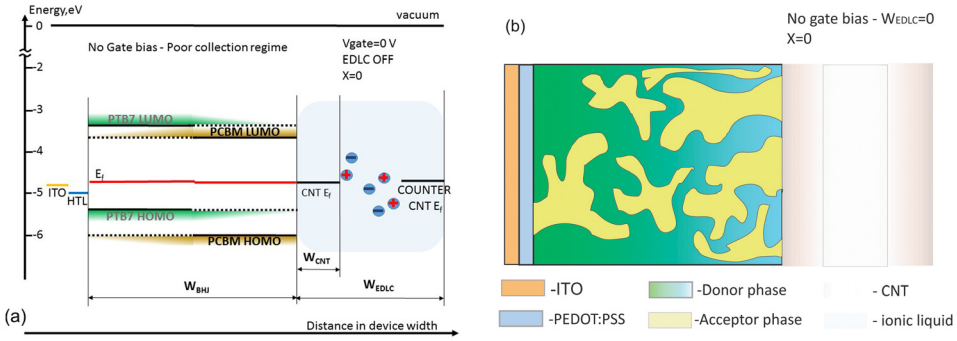

FIG. 13. (a) Band diagram of the back sub-cell at zero Vgate with sketch schematics of EDLC and ion penetration into BHJ. (b) Sketch schematics of back sub-cell BHJ and CNT interface modification.

In summary, as it shown in Figures 13–16, the gating process has different regimes dependent on the Vgate value of each sub-cell. Figs. 22–25 are given in the supplementary material since the processes in the P3HT/PCBM sub-cell are quite similar qualitatively to those in Figs. 13–16. Generally, at first, it is a "Poor collecting regime" at zero V_{gate} without EDLC (Fig. 13). Then comes a "Power increasing regime" (Fig. 14) when e^- injection doping of the CNT is provided in formed EDLC. After this "PEAK POWER" regime starts when the Fermi level of the CNT cathode is raised, E_f equals the PCBM LUMO position. In this case, there is no potential barrier for electron transfer to the PCBM acceptor's LUMO from the CNT conduction band, and as a result, n-type doping of PCBM begins (Fig. 15) with the formation of a local i-n junction within PCBM. A further increase in gating bias shifts the E_f of the CNT further upwards to reach polymer donor's LUMO (Fig. 16), and this process negatively affects the quality of bulk heterojunctions because of the wrong type of electronic e^- injection into donor's LUMO. In this case, the device loses benefits of good exciton photogeneration in the donor polymer (due to the inter-band absorption decrease by absorption shifted to intra-gap bands of polarons in doped donor polymer chains) and output power starts to fall down after peak values of V_{gate} of each sub-cell. The process is presented in the sketch band diagrams and the device scheme with special markings, such as X-n-injection doped layer width, W_{BHJ}—OPV bulk heterojunction width, e.g., 90 nm for the PTB7 sub-cell, W_{CNT}—width of 1 layer of the CNT laminated electrode, and W_{EDLC}—width of the ionic liquid layer (where electric double charging takes place); the semitransparent light grey area schematically presents ionic liquid between the common and counter CNTs.

It should be mentioned that the described regimes are equal for each sub-cell in sequence but not equal to the value of peak V_{gate}. This effect of back sub-cell turning "ON" earlier, i.e., at lower gating potential, compared to the front sub-cell was unexpected as the sub-cells share a common gate and common electrodes (as it is shown in Figures 13–16). The work function

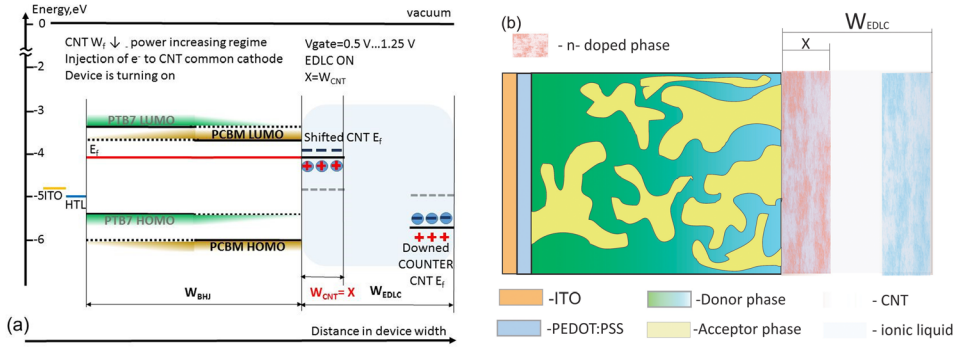

FIG. 14. (a) Band diagram of the back sub-cell in the CNT e^- injection process at 0,5…1,25 V_{gate} with sketch schematics of EDLC and ion penetration into BHJ. (b) Sketch schematics of back sub-cell BHJ and CNT interface modification.

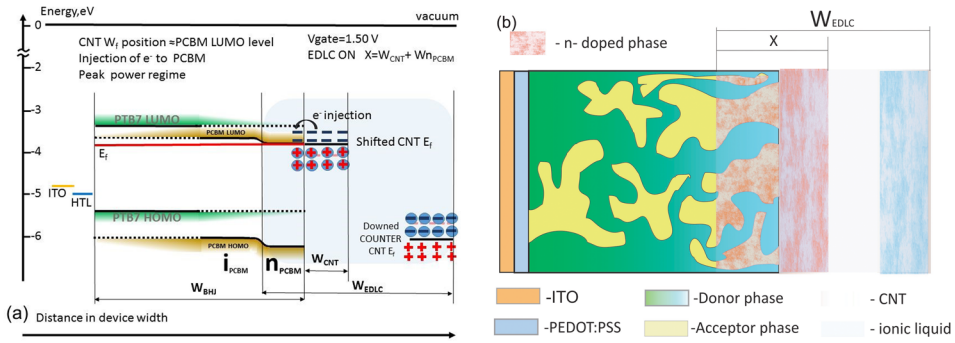

FIG. 15. (a) Band diagram of the back sub-cell in the e^- injection process to the PCBM LUMO level at 1.50 V of V_{gate} with sketch schematics of EDLC and penetration of ions into BHJ. (b) Sketch schematics of back sub-cell BHJ and CNT interface modification upon gate induced n-doping of the PCBM acceptor.

of their cathode, and therefore the degree of electrode asymmetry between the ITO and the cathode, is expected to be identical in a simple qualitative picture. However, the actual experiment demonstrated that it is not correct and that charging of MWCNTs on different sub-cells is not equal. Furthermore, the back sub-cell shows a higher V_{OC} than the front sub-cell and should require greater electrode asymmetry with respect to the work function than the front sub-cell and thus a larger V_{gate} before turning ON (Figure 14).

Given the lower HOMO level of the PTB7 polymer, it is possible that the suppression of hole injection/extraction occurs more rapidly in PTB7, and thus, the device turns ON at a lower V_{gate}. Other effects to consider are the fact that PTB7 is a copolymer, which is a polymer composed of alternating donor (D) and acceptor (A) units. This might have an impact on the interface D-A dipoles generated between the polymer chain and the CNT common electrode. In addition, the device architecture has cell asymmetry because of different BHJ film thicknesses of sub-cells. They are 90 nm and 200 nm for the PTB7 back sub-cell and the P3HT front sub-cell, respectively, which can also be the origin of front sub-cell switching ON delay, caused by higher V_{gate} for the optimal depth of BHJ doping (marked as "X" in Figs. 13–16).

The above described extension of doping from MWCNTs to PCBM and further to polymeric chains should be observed in other phenomena induced by gating, which can be an independent confirmation of the proposed charge injection into PCBM or the polymer (P3HT and/or PTB7) at higher gating voltage. Therefore, we have studied carefully the time dynamics of charging currents, associated with gating, which appear in the ionic gate circuit, after the application of V_{gate}, and below we describe the results of charge injection clearly seen as the new charging current slowly increases.

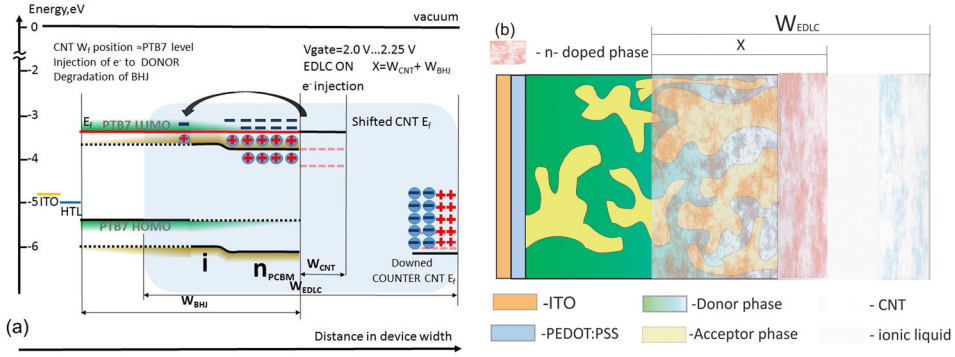

FIG. 16. (a) Band diagram of the back sub-cell in the e^- injection process to the PTB7 donor LUMO level at 2.0 V of V_{gate} with sketch schematics of EDLC and ion penetration into BHJ. (b) Sketch schematics of back sub-cell BHJ and CNT interface modification upon doping of both PCBM and PTB7 layer adjacent to CNTs.

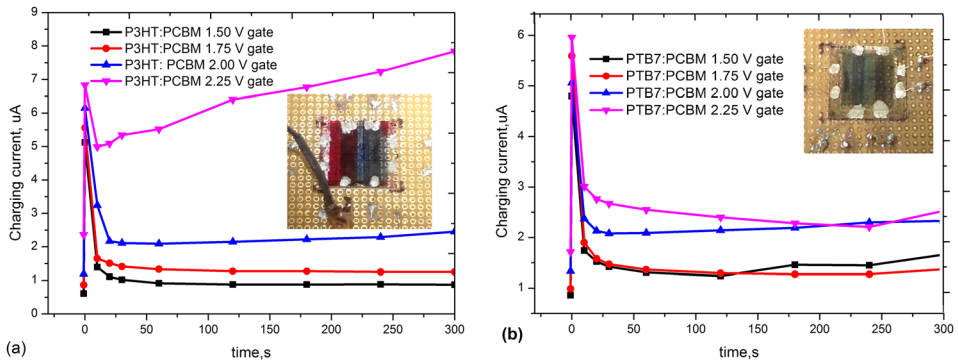

FIG. 17. Time dependence of charging current between MWCNT electrodes in (a) P3HT sub-cells and (b) PTB7 sub-cell and at $V_{gate} < 1.5$ V (a) and $V_{gate} \geq 1.5$ V. The insets in (a) and (b) show the visual color changes at the largest ionic gating V_{gate}, which corresponds to the opto-electrochemical effect of doping induced formation of new polaronic/bipolaronic bands in P3Ht and in PTB7 and decrease of interband absorption.

So, this independent second confirmation of the suggested n-doping process of PCBM (or polymer chains in BHJ) itself at higher gate voltages $V_g > V_{threshold}$ has been indeed observed as the qualitative change in the charging currents I_{ch}. By this method (described in detail in the supplementary material), we observed the time dependent process of double layer charge (EDLC) formation of ions on the surface of MWCNTs and injected carriers (first to the MWCNT and further to PCBM LUMO level). Charging currents versus time curves were measured for P3HT and PTB7 sub-cells separately. The time dependence of characteristic charging current between MWCNT electrodes is presented in the inset in Figures 17(a), 17(b), and 18 (supplementary material), demonstrating two limiting cases. In both the figures, the curves at small V_{gate} show a fast peak followed by fast decay of current (when the ionic gate-capacitor is already charged) to saturated nA level I_{ch}. The curve at large Vgate shows a qualitatively different behavior: a fast charging peak is followed by slower decay after which the second slow increase in current is clearly observed. This second slow charging corresponds to electron injection from the CNT to the LUMO of PCBM, resulting in slow charging of a second capacitor, formed by the CNT counter electrode and the n-doped PCBM network. As seen from different second current raising in the case of P3HT/PCBM and PTB7/PCBM, the charging at even higher V_{gate} extends from PCBM to the donor polymer's LUMO (which is above PCBM). In addition, it should be mentioned that the described tuning effect of output performance can be repeatable at different V_{gate} values. For this step, it is necessary to discharge CNT electrodes to the initial I_{ch} level between them by applying zero voltage on the gate. After that, output performance at different V_{gates} values can be repeated (discharge current graphs presented in the supplementary material with I_{ch} graphs in the full V_{gate} range).

The procedure of ionic gating in parallel tandem devices, described in the text, is applicable not only to polymeric OPV structures but also in principle to any PV (e.g., low molecular OPV or even to currently developing perovskite PVs) if they adhere to the following constraints. The semiconducting photoactive material must not be soluble or adversely affected by the ionic materials (which is unfortunately the case in perovskites, due to their ionic character, and thus dissolution by usual ionic liquids). In the case of light emitting or photovoltaic devices, the anode and semiconducting layers should not be opaque in the same spectral regions. Given these constraints, it is possible to apply these techniques to organic light emitting diodes, organic field effect transistors, and similar inorganic devices.

CONCLUSIONS

In conclusion, a parallel tandem device tunable by ionic gating and its fabrication method that possesses benefits over conventional processing methodologies are described. We have investigated the regimes of low, medium, and high gate voltages. At low Vgate (Vg < 1.5 V

that we have studied earlier in Refs. 35–37), the gate induces the EDLC doping of only the MWCNT interlayer raising its Fermi level, turning CNTs into an electron collecting cathode and thus switching "ON" a photodiode regime that leads to an increased overall Voc. The Isc increases due to better charge collection from both the sub-cells by n-doped CNTs at this small V_{gate}. A Medium V_{gate}, e.g., $1.5\,V < V_{gate} < 2\,V$, is the best ionic gating regime studied here with the example of low band-gap PTB7 and low LUMO acceptor PCBM with MWCNTs. In this regime, the performance of the whole tandem device increases due to the beginning of n-doping of the polymeric PCBM acceptors by charge injection from MWCNTs (when Ef of CNTs reached the LUMO of PCBM), leading to the formation of a favorable ohmic interface between n-CNTs and n-PCBM. Moreover, partial n-doping of PCBM in the interfacial layer close to MWCNTs creates an internal pulling electric field (at the i-n junction with intrinsic PCBM layers), further improving the performance and providing a better FF, and resulting in peak output power. The hypothesis of n-doping of PCBM at higher $V_{gate} > 1.75\,V$ is proven by the observation of the qualitative change in charging current dynamics (described in detail in the supplementary material). Finally, at higher Vgate, above the threshold value, e.g., approximately at $1.75\,V < Vg < 2.25\,V$ (lower limit, depending on the type of polymer, e.g., for PTB7/PCBM sub-cells and MWCNTs), the donor polymer (PTB7 or PHT) is also most probably becoming n-doped, and the optical interband excitonic absorption is decreased due to the appearance of new intra-gap absorption bands (and color change of PTB7) due to the formation of polarons and bipolarons in PTB7 upon its doping.

We have demonstrated that the back sub-cell turns "ON" earlier than the front sub-cell and the latter acts as a shunt since it is still in its "OFF" state and does not generate enough Jsc and Voc. This effect was unexpected as both the sub-cells share the same gate and common electrodes. We can conclude that for parallel tandem devices to approach ideal performance, both the sub-cells must be in the ON state and the FF of each sub-cell must be higher than 0.5.

The dry lamination by dry spin-able MWCNT sheets and ionic gating of MWCNTs require no vacuum processing, it is scalable, can be performed in ambient conditions, and each active layer is fabricated in an optimal manner, reducing the incidence of electrical shorts and simplifying processing. Qualitative key features are identified in the operation of ionically tunable parallel OPV tandem devices. While the overall efficiencies are still somewhat low, further improvements can be made by optimizing photoactive layers and transparency of CNT electrodes. Additionally, if the sub-cell can be turned "ON" at the same time by optimized V_{gate}, tandem η over 8%–10% can be observed.

SUPPLEMENTARY MATERIAL

See supplementary material for experimental details (device fabrication and characterization), explanation and confirmation of n-doping effects, reproducibility, details of discharging processes, and P3HT sub-cell band diagrams with sketch schematics of interface modifications.

ACKNOWLEDGMENTS

Support for this work was provided from the Ministry of Education and Science of the Russian Federation in the framework of Increase Competitiveness Program of NUST "MISiS" (No. K2-2015-014). Partial financial support by Welch Foundation Grant No. AT-1617 is also appreciated. The authors thank William Holmes and J. Bykova for providing CNT forests and Al. Papadimitratos, K. Mielczarek, and J. Velten for technical assistance and useful discussions.

[1]S. Zhang, L. Ye, and J. Hou, "Breaking the 10% efficiency barrier in organic photovoltaics: Morphology and device optimization of well-known PBDTTT polymers," Adv. Energy Mater. **6**, 1502529 (2016).
[2]W. Cao and J. Xue, "Recent progress in organic photovoltaics: Device architecture and optical design," Energy Environ. Sci. **7**, 2123–2144 (2014).
[3]See http://pv.energytrend.com/news/OPV_Cells_New_Efficiency_Record_11_84_percent.html for Press release.
[4]P. Romero-Gómez, F. Pastorelli, P. Mantilla-Pérez, M. Mariano, A. Martínez-Otero, X. Elias, R. Betancur, and J. Martorell, "Semi-transparent polymer solar cells," J. Photonics Energy **5**, 057212 (2015).

[5]K.-S. Chen, J.-F. Salinas, H.-L. Yip, L. Huo, J. Hou Alex, and K.-Y. Jen, "Semi-transparent polymer solar cells with 6% PCE, 25% average visible transmittance and a color rendering index close to 100 for power generating window applications," Energy Environ. Sci. **5**, 9551 (2012).
[6]Z. M. Beiley, M. Greyson Christoforo, P. Gratia, A. R. Bowring, P. Eberspacher, G. Y. Margulis, C. Cabanetos, P. M. Beaujuge, A. Salleo, and M. D. McGehee, "Semi-transparent polymer solar cells with excellent sub-bandgap transmission for third generation photovoltaics," Adv. Mater. **25**, 7020–7026 (2013).
[7]Y. Yuan, J. Huang, and G. Li, "Intermediate layers in tandem organic solar cells," Green **1**(1), 65–80 (2011).
[8]J. You, L. Dou, Z. Hong, G. Li, and Y. Yang, "Recent trends in polymer tandem solar cells research," Prog. Polym. Sci. **38**, 1909–1928 (2013).
[9]T. Ameri, N. Li, and C. J. Brabec, "Highly efficient organic tandem solar cells: A follow up review," Energy Environ. Sci. **6**, 2390 (2013).
[10]T. T. Larsen-Olsen *et al*., "Roll-to-roll processed polymer tandem solar cells partially processed from water," Solar Energy Materials & Solar Cells **97**, 43–49 (2012).
[11]J. Y. Kim *et al*., "Efficient tandem polymer solar cells fabricated by all-solution processing," Science **317**(5835), 222–225 (2007).
[12]B. Yu, F. Zhu, H. Wang, G. Li, and D. Yan, "All-organic tunnel junctions as connecting units in tandem organic solar cell," J. Appl. Phys. **104**(11), 114503 (2008).
[13]R. Schueppel *et al*., "Controlled current matching in small molecule organic tandem solar cells using doped spacer layers," J. Appl. Phys. **107**(4), 044503 (2010).
[14]M. Hiramoto, M. Suezaki, and M. Yokoyama, "Effect of thin gold interstitial-layer on the photovoltaic properties of tandem organic solar cell," Chem. Lett. **19**(3), 327–330 (1990).
[15]J. Xue, S. Uchida, B. P. Rand, and S. R. Forrest, "Asymmetric tandem organic photovoltaic cells with hybrid planar-mixed molecular heterojunctions," Appl. Phys. Lett. **85**(23), 5757 (2004).
[16]Z. Yin, J. Wei, and Q. Zheng, "Interfacial materials for organic solar cells: Recent advances and perspectives," Adv. Sci. **3**, 1500362 (2016).
[17]M. Raïssi, S. Vedraine, R. Garuz, T. Trigaud, and B. Ratier, "Solution processed cathode and interconnecting layer of silver nanowires in an efficient inverted tandem organic solar cells," Sol. Energy Mater. Sol. Cells **160**, 494–502 (2017).
[18]A. F. Mitul *et al*., "Low temperature efficient interconnecting layer for tandem polymer solar cells," Nano Energy **11**, 56–63 (2015).
[19]K.-S. Lee, I. Kim, C. Bong Yeon, J. Wook Lim, S. Jin Yun, and G. E. Jabbour, "Thin metal electrodes for semitransparent organic photovoltaics," ETRI J. **35**(4), 587–593 (2013).
[20]S. Tanaka *et al*., "Monolithic parallel tandem organic photovoltaic cell with transparent carbon nanotube interlayer," Appl. Phys. Lett. **94**(11), 113506 (2009).
[21]K. Mielczarek, A. Cook, A. Kuznetsov, and A. Zakhidov, "OPV tandems with CNTS: Why are parallel connections better than series connections," in *Low-Dimensional Functional Materials* (Springer Science+Business Media, New York, NY, 2013), pp. 179–204.
[22]A. A. Kuznetsov, "Physics of electron field emission by self-assembled carbon nanotube arrays," Ph.D. thesis (The University of Texas at Dallas, 2008).
[23]S. Lee, T. Eui Kang, D. Han, H. Kim, B. J. Kim, J. Lee, and S. Yoo, "Polymer/small-molecule parallel tandem organic solar cells based on MoOx–Ag–MoOx intermediate electrodes," Sol. Energy Mater. Sol. Cells **137**, 34–43 (2015).
[24]H. Yoon Han, H. Yoon, and C. S. Yoon, "Parallel polymer tandem solar cells containing comb-shaped common electrodes," Sol. Energy Mater. Sol. Cells **132**, 56–66 (2015).
[25]S. Bong Lee, S. Cheol Yoon, P. Seok Kim, S. Park, J. Lim, and C. Sup Yoon, "Polymer-based parallel tandem solar cells with a transparent ferroelectric interconnecting layer," Appl. Phys. Lett. **104**, 083302 (2014).
[26]Y. Zheng *et al*., Synth. Met. **221**, 179–185 (2016).
[27]G. Robert *et al*., Proc. SPIE **8830**, 88300I (2013).
[28]P. Mantilla-Perez, A. Martinez-Otero, P. Romero-Gomez, and J. Martorell, ACS Appl. Mater. Interfaces **7**, 18435–18440 (2015).
[29]I. Etxebarria, A. Furlan, J. Ajuria, F. W. Fecher, M. Voigt, C. J. Brabec, M. M. Wienk, L. Slooff, S. Veenstra, J. Gilot, and R. Pacios, "Series vs parallel connected organic tandem solar cells: Cell performance and impact on the design and operation of functional modules," Sol. Energy Mater. Sol. Cells **130**, 495–504 (2014).
[30]J. Jo, J.-R. Pouliot, D. Wynands, S. D. Collins, J. Young Kim, T. Luan Nguyen, H. Young Woo, Y. Sun, M. Leclerc, and A. J. Heeger, "Enhanced efficiency of single and tandem organic solar cells incorporating a diketo pyrrolo pyrrole-based low-bandgap polymer by utilizing combined ZnO/polyelectrolyte electron-transport layers," Adv. Mater. **25**, 4783–4788 (2013).
[31]W. Jose da Silva, F. Kurt Schneider, A. Rashid bin Mohd Yusoff, and J. Jang, "High performance polymer tandem solar cell," Sci. Rep. **5**, 18090 (2015).
[32]M. Raissi, L. Vignau, E. Cloutet, and B. Ratier, "Soluble carbon nanotubes/phthalocyanines transparent electrode and interconnection layers for flexible inverted polymer tandem solar cells," Org. Electron. **21**, 86–91 (2015).
[33]A. A. Kuznetzov, S. B. Lee, M. Zhang, R. H. Baughman, and A. A. Zakhidov, "Electron field emission from transparent multiwalled carbon nanotube sheets for inverted field emission displays," Carbon **48**(1), 41–46 (2010).
[34]A. A. Zakhidov and D.-S. Suh *et al*., "Electrochemically tuned properties for electrolyte-free carbon nanotube sheets," Adv. Funct. Mater. **19**(14), 2266–2272 (2009).
[35]A. Cook, J. D. Yuen, and A. Zakhidov, "Ion-reconfigurable photovoltaic cells, hybrid tandems and photodetectors with CNT ionic gate," U.S. patent application 61,732,379 (2012).
[36]A. B. Cook, J. D. Yuen, and A. Zakhidov, "Electrochemically gated organic photovoltaic with tunable carbon nanotube cathodes," Appl. Phys. Lett. **103**(16), 163301 (2013).
[37]A. B. Cook, J. D. Yuen, J. W. Micheli, A. G. Nasibulin, and A. Zakhidov, "Ambient method for the production of an ionically gated carbon, nanotube common cathode in tandem organic solar cells," J. Vis. Exp. (93), e52380 (2014).
[38]P. Wadhwa, B. Liu, M. A. McCarthy, Z. Wu, and A. G. Rinzler, "Electronic junction control in a nanotube-semiconductor Schottky junction solar cell," Nano Lett. **10**(12), 5001–5005 (2010).

[39]A. B. Cook, Ph.D. thesis, UT Dallas, 2015.
[40]R. H. Baughman, A. A. Zakhidov, and W. A. de Heer, "Carbon nanotubes – The route towards applications," Science **297**, 787–792 (2002).
[41]M. Zhang, S. Fang, A. A. Zakhidov, S. B. Lee, A. Aliev, C. Williams, K. Atkinson, and R. H. Baughman, "Strong, transparent, multifunctional, carbon nanotube sheets," Science **309**, 1215 (2005).
[42]R. Ulbricht, S. B. Lee, X. M. Jiang, K. Inoue, M. Zhang, S. Fang, R. H. Baughman, and A. A. Zakhidov, "Transparent carbon nanotube sheets as 3-D charge collectors in organic solar cells," Sol. Energy Mater. Sol. Cells **91**(5), 416–419 (2007).
[43]C. D. Williams, R. Ovalle Robles, M. Zhang, S. Li, R. H. Baughman, and A. A. Zakhidov, "Multiwalled carbon nanotube sheets as transparent electrodes in high brightness organic light-emitting diodes," Appl. Phys. Lett. **93**, 183506 (2008).